

Unit Circle Rectification of the MVDR Beamformer

Saurav R. Tuladhar, John R. Buck, *Senior Member, IEEE*

Abstract

The sample matrix inversion (SMI) beamformer implements Capon's minimum variance distortionless (MVDR) beamforming using the sample covariance matrix (SCM). In a snapshot limited environment, the SCM is poorly conditioned resulting in a suboptimal performance from the SMI beamformer. Imposing structural constraints on the SCM estimate to satisfy known theoretical properties of the ensemble MVDR beamformer mitigates the impact of limited snapshots on the SMI beamformer performance. Toeplitz rectification and bounding the norm of weight vector are common approaches for such constraints. This paper proposes the unit circle rectification technique which constrains the SMI beamformer to satisfy a property of the ensemble MVDR beamformer: for narrowband planewave beamforming on a uniform linear array, the zeros of the MVDR weight array polynomial must fall on the unit circle. Numerical simulations show that the resulting unit circle MVDR (UC MVDR) beamformer frequently improves the suppression of both discrete interferers and white background noise compared to the classic SMI beamformer. Moreover, the UC MVDR beamformer is shown to suppress discrete interferers better than the MVDR beamformer diagonally loaded to maximize the SINR.

Index Terms

adaptive beamformer, MVDR, Capon beamformer, array polynomial, unit circle

I. INTRODUCTION

Adaptive beamformers in practical settings face the challenge of extracting enough information from a limited set of observations, or snapshots, to suppress discrete interferers while maintaining attenuation of background white noise. The motion of sources enforces a limit on the number of snapshots which can be coherently combined [1]. Imposing structural constraints on the covariance matrix or array weights forces a beamformer to satisfy known theoretical properties of the ensemble covariance matrix (ECM), making the best use of the limited information available in snapshot poor scenarios. Common approaches for such constraints include Toeplitz rectification [2]–[6], and limiting the norm of the weight vector [7]. Imposing an upper bound on the norm of the weight vector ensures a minimum amount of white noise gain while also providing robustness to mismatch in sensors' locations or gains [8]. In the spirit of such constraints, this paper proposes a new rectification technique for mitigating the impact of limited snapshots on the performance of Capon's minimum variance distortionless response (MVDR) beamformer [9] - the unit circle rectification.

The unit circle rectification constrains the MVDR beamformer weights to satisfy a property first observed by Steinhart and Guerci: for a narrowband planewave MVDR beamformer on a uniform linear array (ULA), the zeros of the z -transform of the conjugated array weights must fall on the unit circle [10]. The polynomial resulting from this z -transform is known as the *array polynomial* [11]. This unit circle property observed by Steinhart and Guerci holds for the case of the ensemble MVDR beamformer. However, the zeros of the array polynomial of the practical sample matrix inversion (SMI) beamformer generally do not fall on the unit circle. The unit circle rectification enforces consistency with the unit circle property by projecting the zeros of the SMI beamformer array polynomial back to the unit circle [12]. The projection can be considered as an alternative method of conditioning the beamformer weights, similar in spirit but complementary to Toeplitz rectification [2]–[6]. Enforcing this consistency moves the SMI solution closer to the ideal ensemble solution, improving the performance of the practical adaptive beamformer.

This paper focuses on transferring intuition about the z -transform and the frequency response in time-domain linear systems to the array polynomial and beampattern in spatial processing, rather than rigorous

performance proofs. Monte Carlo simulations for small and large arrays for several snapshot regimes confirm the benefits of transferring this intuition across domains. The resulting unit circle MVDR (UC MVDR) beamformer is remarkable in that simulation results show that for the snapshot limited scenarios studied here, it frequently improves the suppression of both discrete interferers and white background noise relative to the classic SMI solution.

The remainder of this paper is organized as follows: Sec. II reviews planewave beamforming and establishes the notation followed in the sequel. Sec. III develops the array polynomial representation for narrowband beamformers using ULAs. Sec. IV presents the unit circle rectification technique used to derive the UC MVDR beamformer. Sec. V discusses the simulation results comparing the performance of the UC MVDR beamformer against the SMI beamformer and the diagonal loaded MVDR beamformer. Sec. VI discusses the limitations of the proposed unit circle rectification technique and the potential directions for future enhancement. Sec. VII presents the concluding remarks.

II. PLANEWAVE BEAMFORMING

This section presents a brief review on planewave beamforming to establish the notation used in this paper. A comprehensive discussion on planewave beamforming and related topics can be found in the classical texts [13], [14].

The narrowband planewave data measured with an N sensor ULA is represented as an $N \times 1$ vector of complex phasors \mathbf{x} or a snapshot, commonly modeled as,

$$\mathbf{x} = \sum_{i=1}^D a_i \mathbf{v}_i + \mathbf{n}, \quad (1)$$

where D is the number of planewave signals, a_i is i^{th} signal amplitude, \mathbf{v}_i is the planewave array manifold vector for the i^{th} signal, and \mathbf{n} is the additive noise vector. The amplitudes are modeled as a zero mean complex circular Gaussian random variable, i.e., $a_i \sim \mathcal{CN}(0, \sigma_i^2)$ and the background noise is assumed to be spatially white with complex circular Gaussian distribution, i.e., $\mathbf{n} \sim \mathcal{CN}(\mathbf{0}, \sigma_w^2 \mathbf{I})$. The array manifold vector is a complex exponential vector

$$\mathbf{v}_i = [1, e^{-j(2\pi u_i/\lambda)d}, e^{-j(2\pi u_i/\lambda)2d}, \dots, e^{-j(2\pi u_i/\lambda)(N-1)d}]^T,$$

where $u_i = \cos(\theta_i)$ and θ_i is the i^{th} signal direction, λ is the wavelength, d is the inter-sensor spacing on the ULA and $[\cdot]^T$ denotes transpose. In the sequel, the signal direction will be represented in terms of the directional cosine u . Assuming the D signals in (1) are uncorrelated, the data ECM is

$$\Sigma = E[\mathbf{x}\mathbf{x}^H] = \sum_{i=1}^D \sigma_i^2 \mathbf{v}_i \mathbf{v}_i^H + \sigma_w^2 \mathbf{I}, \quad (2)$$

where σ_i^2 is i^{th} signal power and σ_w^2 is the sensor level noise power. The ECM quantifies the statistical relation between the data measured at each pair of sensors.

Beamformers spatially filter the array data by passing the signal from select look directions while rejecting noise and interfering signals. The beamformer output (y) is obtained as the weighted sum of the sensor data, i.e. $y = \mathbf{w}^H \mathbf{x}$, where \mathbf{w} is the $N \times 1$ complex array weight vector. The conventional beamformer (CBF) is the basic beamformer whose weights shift signals measured at each sensor such that planewave signals from the look direction u_0 align in time and combine constructively while signals from other directions combine destructively and are suppressed. A CBF steered to the look direction $u_0 = \cos(\theta_0)$ has a weight vector equal to the array manifold vector for the look direction normalized for unit gain, i.e., $\mathbf{w}_{\text{CBF}} = \mathbf{v}_0/N$.

The choice of weights determines the beamformer's beampattern. The beampattern $B(u)$ defines the complex gain due to the beamformer for a unit amplitude planewave from direction $u = \cos(\theta)$, i.e.,

$$B(u) = \mathbf{w}^H \mathbf{v}(u) = \sum_{n=0}^{N-1} w_n^* \left(e^{-j \frac{2\pi u}{\lambda} d} \right)^n \quad (3)$$

where $(\cdot)^*$ denotes conjugate and $-1 \leq u \leq 1$ is the directional cosine. The beampattern is analogous to the frequency response of a discrete-time (DT) linear system. The beampattern magnitude $|B(u)|$ is characterized by a mainlobe in the look direction (u_0) and the multiple sidelobes outside the mainlobe. The beampattern magnitude squared in the interferer direction is the notch depth (ND), i.e., $\text{ND} = |B(u_I)|^2$, where u_I is the interferer direction. The ND quantifies the interferer attenuation due to the beamforming.

White noise gain quantifies the improvement in SNR due to the beamformer suppressing the spatially-white background noise. Assuming unity gain in the look direction i.e., $B(u_0) = 1$, white noise gain (WNG) is given by $\text{WNG} = \|\mathbf{w}\|^{-2}$ where $\|\cdot\|$ denotes the Euclidean norm [13]. WNG is also a metric for beamformer robustness against mismatch [8]. For a given ULA, the CBF has the maximum WNG which is equal to the number of array elements N [7].

A. MVDR beamformer

Capon proposed the MVDR beamformer as an optimum adaptive beamformer (ABF) [9]. The MVDR beamformer minimizes the output variance $E(|y|^2) = \mathbf{w}^H \Sigma \mathbf{w}$ while maintaining unity gain in the look direction with the array manifold vector \mathbf{v}_0 . The MVDR weight vector \mathbf{w}_{MVDR} is derived as the solution to the constrained optimization problem

$$\min_{\mathbf{w}} f(\mathbf{w}) = \mathbf{w}^H \Sigma \mathbf{w} \quad \text{s.t.} \quad \mathbf{w}^H \mathbf{v}_0 = 1, \quad (4)$$

where Σ is the interferer-plus-noise ECM and \mathbf{v}_0 is the array manifold vector for the look direction $u_0 = \cos(\theta_0)$. The optimal solution is

$$\mathbf{w}_{\text{MVDR}} = \frac{\Sigma^{-1} \mathbf{v}_0}{\mathbf{v}_0^H \Sigma^{-1} \mathbf{v}_0}. \quad (5)$$

Computing the MVDR weights in (5) requires knowledge of the ECM but in practical applications the ECM is unknown. Consequently, the MVDR beamformer is approximated by the SMI beamformer by replacing the ECM Σ in (5) with the SCM,

$$\mathbf{S} = \frac{1}{L} \sum_{l=1}^L \mathbf{x}_l \mathbf{x}_l^H$$

where the L is the number of data snapshots and \mathbf{x}_l is the l^{th} data snapshot vector defined in (1). The SMI beamformer is the simplest practical implementation of the MVDR beamformer.

The SMI beamformer relies on the availability of a large number of snapshots (L) such that $L \gg N$, where N is the number of sensors. The SCM computed from sufficiently large L gives an accurate estimate of the ECM [15]. Reed et al. show that at least two snapshots per sensor, i.e., $L \geq 2N$ is required to ensure that the expected output SINR loss due to the use of the SCM instead of the ECM is 3 dB or less [16]. In many beamforming scenarios, physical non-stationarities in the environment or source locations preclude averaging large numbers of snapshots to form the SCM. The use of long arrays and the presence of fast moving sources severely limit the available number of snapshots. In many passive sonar applications it is common to have only limited snapshots ($L \approx N$) or even insufficient snapshots ($L < N$) available and even two snapshots per sensor ($L = 2N$) is considered a snapshot rich case [1], [17]. When the number of snapshots are limited ($L \approx N$) the SCM is ill-conditioned and the SCM inversion is numerically unstable. Inadequate estimation of the SCM results in high sidelobes and distorted mainlobe in the beampattern and subsequent degradation in interferer and white noise attenuation [18], [19]. Moreover, in the snapshot

deficient case $L < N$, the SCM is rank deficient and the SCM inversion is not possible. This paper focuses on the limited snapshot scenarios with $L \leq 2N$.

A common approach to address the limited snapshot scenario is to apply diagonal loading (DL) to the SCM to get $\mathbf{S}_\delta = \mathbf{S} + \delta \mathbf{I}$, where δ is the DL factor [13]. The DL MVDR beamformer weights are computed by replacing the ECM in (5) with the DL SCM \mathbf{S}_δ . DL makes the SCM inversion numerically stable, provides better sidelobe control and improves the beamformer WNG while introducing bias [20]–[22].

However, choosing the best loading factor to combat the impact of limited snapshots in a practical scenario remains a challenging problem. Several ad-hoc approaches have been proposed for choosing the appropriate DL factor: $\delta = 10\sigma^2$ where σ^2 is the noise power [23], $\delta = -\hat{\lambda}_{\min} + \sqrt{(\hat{\lambda}_D - \hat{\lambda}_{\min})(\hat{\lambda}_{D+1} - \hat{\lambda}_{\min})}$ where $\hat{\lambda}_{\max} = \hat{\lambda}_1 \geq \dots \geq \hat{\lambda}_N = \hat{\lambda}_{\min}$ are the sample eigenvalues and D is dimension of the interferer subspace. These methods require knowledge of the noise power level and interferer subspace dimension which are unknown in practice. Other ad-hoc considerations for the choice of diagonal loading have been proposed as summarized in [24, Sec:III].

In contrast, Mestre and Lagunas systematically optimized the DL factor to maximize the SINR to derive a random matrix theory based optimal DL factor estimator for snapshot limited scenarios [21]. The authors derive an expression relating the asymptotic output SINR to the DL factor δ and the ratio of snapshots per sensor. The optimal DL factor is the solution that maximizes the output SINR. However, the procedure to search for the optimal DL factor has a significantly higher computational complexity compared to ad-hoc procedures.

III. ARRAY POLYNOMIALS

The array polynomial is the z -transform of the conjugated array weights of a narrowband beamformer for a ULA [11], [13], [25]. The array polynomial is analogous to the system function representation of a DT linear system obtained by taking the z -transform of the system impulse response. As with DT linear systems, beamformers also have a pole-zero representation in the complex plane. Continuing the analogy, the beampattern is obtained by evaluating the array polynomial along the unit circle $\{z \in \mathbb{C}, |z| = 1\}$.

The beampattern of a narrowband beamformer using a ULA can be represented as a complex polynomial [11][25]. Letting $d = \lambda/2$ and $z = e^{j\pi u}$ in (3) yields the array polynomial

$$P(z) = \sum_{n=0}^{N-1} w_n^* z^{-n} = \mathcal{Z}(\mathbf{w}^H). \quad (6)$$

where $\mathcal{Z}()$ is the z -transform operator and $*$ denotes the complex conjugate operator. $P(z)$ is an $N - 1$ degree polynomial in complex variable z with the conjugated complex beamformer weights (w_n^*) as coefficients. Eq. (6) is the z -transform of the conjugated beamformer weights [26, Chap. 3]. The array polynomial representation maps the bearing variable u into the complex plane. The phase of the complex variable (z) is related to the cosine bearing variable u as $\arg(z) = \pi u$. In the complex plane, the array polynomial has $N - 1$ zeros and the corresponding $N - 1$ poles are all at the origin. Evaluating (6) on the unit circle $\{z \in \mathbb{C}, |z| = 1\}$ yields the beampattern. The zeros of the array polynomial correspond to the beampattern notches and when the zeros fall on the unit circle they result in perfect notches or *nulls* in the beampattern.

A CBF using an N sensor ULA and steered to the broadside ($u_0 = 0$) look direction has a weight vector $\mathbf{w}_{\text{CBF}} = \mathbf{1}/N$ where $\mathbf{1}$ is a vector of N ones. Applying the array polynomial approach to the CBF finds the classic finite geometric series result from linear system theory, possibly shifted in angle based on the look direction. The z -transform of \mathbf{w}_{CBF} gives the CBF polynomial

$$P_C(z) = \frac{1}{N} \sum_{n=0}^{N-1} z^{-n} = \frac{1}{N} \left[\frac{z^N - 1}{z^{N-1}(z - 1)} \right]. \quad (7)$$

When $P_C(z)$ is evaluated on the unit circle, the finite geometric series can be manipulated into the well-known discrete sinc function, with a main lobe in the look direction [26, Chap. 3]. The CBF polynomial zeros are the roots of the numerator in (7), which are the N roots of unity. These roots give equally spaced zeros on the unit circle except for the root at $z = 1$ which is canceled by a corresponding pole. Hence, a CBF using an N sensor ULA has $N - 1$ zeros confined onto the unit circle and these zeros produce the nulls in the CBF beampattern [13].

A. MVDR array polynomial

Following the definition in (6), the ensemble MVDR beamformer array polynomial is $P_M(z) = \mathcal{Z}(\mathbf{w}_{\text{MVDR}}^H)$. Factoring the polynomial,

$$P_M(z) = \Gamma \prod_{n=1}^{N-1} (1 - \zeta_n z^{-1}),$$

where Γ is a scaling term and ζ_n is the n^{th} zero of the ensemble MVDR beamformer array polynomial (or "ensemble zero" for brevity in the sequel). Fig. 1 shows the ensemble zeros and beampattern for an example case of the MVDR beamformer using an $N = 11$ sensor ULA. A single interferer is present at $u_I = 3/N$ and the interferer-to-noise power ratio (INR) is 10 dB. The dashed radial line in Fig. 1a indicates the angle πu_I corresponding to the interferer direction u_I denoted by the vertical dashed line in Fig. 1b. All $N - 1$ ensemble zeros in Fig. 1a are on the unit circle and these zeros correspond to the beampattern nulls in Fig. 1b. However, the beampattern nulls are not necessarily in the interferer direction. The interferer ND depends on the INR level. The objective function in (4) requires that the MVDR beamformer minimizes the total output power. As the INR changes, the MVDR beamformer adapts the ND and the WNG to reduce the total output power. This behavior manifests in the form of MVDR polynomial zeros shifting along the unit circle as the INR changes. Numerical experiments show that the MVDR beamformer controls the interferer suppression by placing a beampattern notch such that the interferer falls on the shoulder of the notch. As INR increases, the zeros shift along the unit circle towards the interferer direction yielding a deeper notch. As INR decreases, the zeros shift away from the interferer direction yielding a shallower notch. In fact the MVDR ensemble zeros are always located on the unit circle for planewave beamforming using ULAs. Steinhardt and Guerci [10] first proved this unit circle property for the ensemble MVDR beamformer, though their result does not seem to be widely known. Appendix A outlines their proof of the unit circle property.

In practice, each realization of the SMI MVDR beamformer has an array polynomial representation defined as $P_S = \mathcal{Z}(\mathbf{w}_{\text{SMI}}^H)$. The zeros of the SMI MVDR weights array polynomial (or "sample zeros" in the sequel) are randomly perturbed from the ensemble zero locations on the complex plane. Fig. 2 is a composite of sample zeros (green markers) obtained from 1000 independent realizations of the SMI MVDR beamformer. It considers an example case of a $N = 11$ sensor ULA using $L = 10N$ snapshots to compute the SCM and a single interferer present $u_I = 3/N$ with INR = 40 dB. The number of snapshots is impractically large for many passive sonar situations, but is chosen to create a clearer clustering of the sample zeros around the ensemble zeros. Examining Fig. 2 shows the sample zeros clustering around the ensemble zero locations ζ_n while not necessarily falling on the unit circle. The SMI MVDR beampattern converges in probability to the ensemble beampattern as the number of snapshots L increases [27]. Thus the sample zeros also converge to ensemble zero locations as the number of snapshot increases.

Continuing the analogy with DT LTI systems, the sample zeros that fall away from the unit circle correspond to shallow notches instead of nulls in SMI MVDR beampattern. Further, any zeros that fall closer to the origin or far outside the unit circle have negligible contribution to beampattern [26, Chap. 5]. Hence the SMI MVDR beamformer suffers from beampattern distortion resulting in loss of interferer suppression and WNG. The following section describes how the SMI MVDR beamformer can be modified to improve interferer suppression by moving the sample zeros to the unit circle.

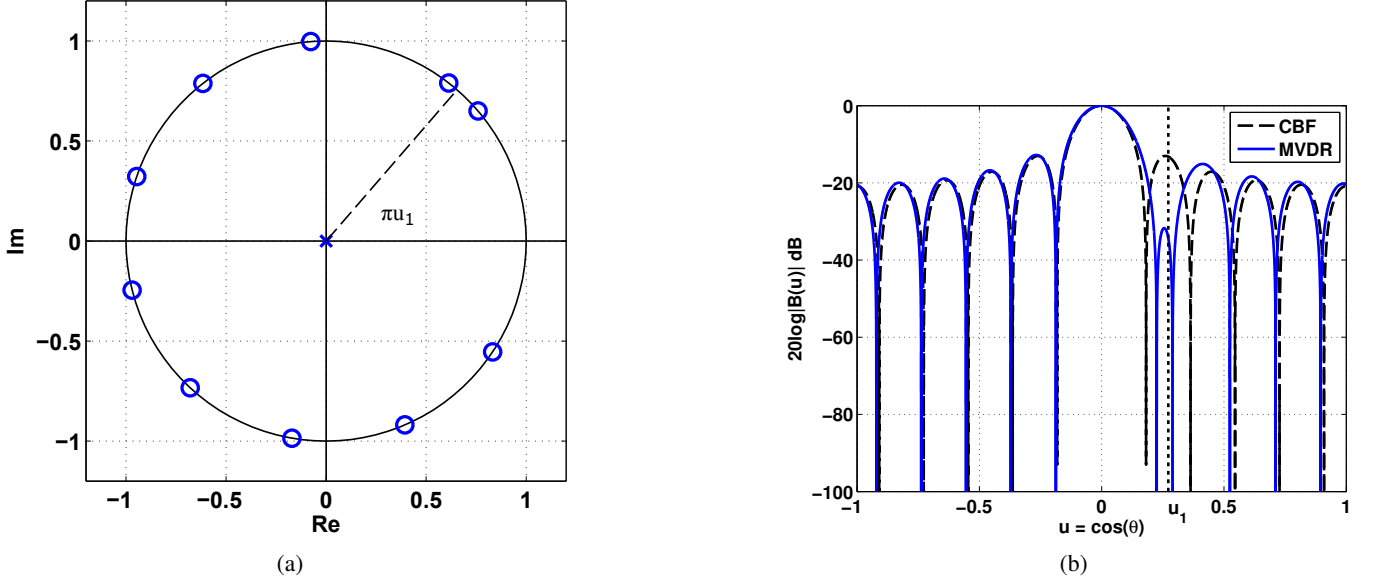


Fig. 1. MVDR beamformer (a) zero locations and (b) beampattern for an example case using $N = 11$ sensor ULA and a single interferer at $u_1 = 3/N$ indicated by vertical dashed line in (b). In (a) the dashed line at πu_1 indicates the angle in the complex plane corresponding to the interferer.

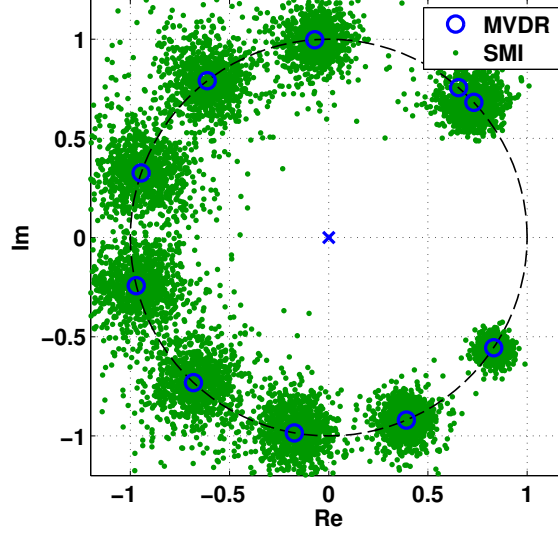


Fig. 2. SMI MVDR zeros from 1000 Monte Carlo trials for $N = 11$, $L = 10N$ and $\text{INR} = 40$ dB. The number of snapshots is impractically large for many passive sonar situations, but makes clear the clustering of the SMI zeroes around the ensemble zeroes.

IV. UNIT CIRCLE RECTIFICATION

The unit circle rectification algorithm projects the sample zeros radially to the unit circle, enforcing the unit circle property of the ensemble MVDR polynomial zeros. Applying the unit circle rectification to the SMI beamformer produces the UC MVDR beamformer. The zeros on the unit circle guarantee nulls in the UC MVDR beampattern in the directions corresponding to the sample zeros. The rest of the section describes the unit circle rectification to derive the UC MVDR beamformer assuming the beamformer is steered towards the broadside ($u_0 = 0$). The algorithm extends naturally to the case of a different look direction ($u_0 = u_L$) by changing the array manifold vector used for the SMI beamformer, and then shifting the mainlobe exclusion region for zeros described below.

Algorithm 1 outlines the UC MVDR beamformer implementation. The algorithm begins from the SMI MVDR weights \mathbf{w}_{SMI} . The z -transform of the conjugated weights gives the SMI MVDR polynomial

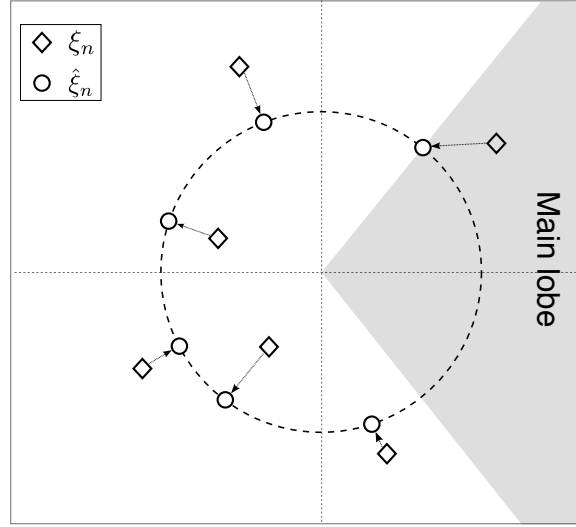


Fig. 3. Schematic shows the unit circle projection technique. The diamond markers denote the sample zeros (ξ_n) and the circle markers denote the unit circle zeros ($\hat{\xi}$) obtained by radially projecting the sample zeros. The sample zeros within the main-lobe region ($-2/N \leq u \leq 2/N$) are moved to the closest CBF first-null location ($u_{\text{null}} = \pm 2/N$) on the unit circle.

$P_S(z) = \mathcal{Z}(\mathbf{w}_{\text{SMI}}^H)$. Factoring the SMI MVDR polynomial,

$$P_S(z) = G \prod_{n=1}^{N-1} (1 - \xi_n z^{-1}),$$

where G is the gain required to ensure unity gain in the look direction ($u_0 = 0$), i.e., $P_S(e^{j\pi u_0}) = 1$ and $\xi_n = r_n e^{j\omega_n}$ is the n^{th} SMI MVDR polynomial zero. As previously discussed in Sec. III-A, the sample zeros are not necessarily on the unit circle and hence the magnitudes $|\xi_n| = r_n$ of the roots are generally not unity. The next step is to radially project the SMI MVDR polynomial zeros ξ_n to the unit circle, which is essentially the unit circle rectification. Fig. 3 illustrates the projection of the sample zeros (diamond markers) to the unit circle zeros (circle markers). Projection yields a set of unit circle zeros $\hat{\xi}_n = e^{j\omega_n}$. An exception occurs when the sample zeros fall within the CBF main-lobe region in the complex plane i.e. $|\arg(\xi_n) - \pi u_0| < 2\pi/N$. Projecting such zeros radially to the unit circle results in nulls inside the main-lobe of the UC MVDR ABF. A null inside the main-lobe results in undesired main-lobe distortion and drastic loss in WNG [13, Sec. 6.3.1]. Rather than radially projecting to the unit circle, such zeros are moved to the closest CBF first-null location on the unit circle such that $\arg(\hat{\xi}_n) = \text{sgn}(\omega_n)2\pi/N$ where $\text{sgn}(\cdot)$ is the sign function. This exclusion strategy is functionally similar to other main-lobe protection schemes for adaptive beamformers use to avoid deep notches in the main lobe too close to the look direction, e.g., [28]–[30]. The UC MVDR approach differs in manipulating the main-lobe nulls in terms of the locations of the array polynomial roots rather than the inner product of the look direction replica vector with the SCM eigenvectors.

The projected unit circle zeros $\hat{\xi}_n$ are used to synthesize a unit circle polynomial

$$P_{UC}(z) = \prod_{n=1}^{N-1} \frac{(1 - \hat{\xi}_n z^{-1})}{(1 - \hat{\xi}_n)}. \quad (8)$$

Rewriting the polynomial in terms of the coefficients

$$P_{UC}(z) = \sum_{n=0}^{N-1} c_n^* z^{-1}. \quad (9)$$

Comparing (9) to the definition of the array polynomial (6), the coefficients c_n s can be viewed as beamformer weights. Thus, the UC MVDR ABF weight vector is defined as $\mathbf{w}_{UC} = [c_1, c_2, \dots, c_N]^T$. The denominator of $(1 - \hat{\xi}_n)$ in (8) guarantees that the coefficients c_n sum to 1, and thus satisfy the unity gain constraint on the broadside look direction ($u_0 = 0$) we are assuming here. Evaluating $P_{UC}(z)$ on the unit circle produces the UC MVDR ABF beampattern with $N - 1$ nulls in the directions corresponding to $\hat{\xi}_n$'s and a unity gain in the look direction, i.e., $P_{UC}(e^{j\pi u_0}) = 1$.

Fig. 4 shows a representative example comparing the UC MVDR and the SMI MVDR ABF using an $N = 11$ sensor ULA and $L = 12$ snapshots. Both ABFs are steered to broadside ($u_0 = 0$) look direction and a single interferer is present at $u_I = \cos(\theta_I) = 3/N$ with power 40 dB above the background white noise. In Fig. 4a, the blue diamond markers indicate the sample zero locations and the magenta circle markers indicate the UC MVDR zeros projected on unit circle. Fig. 4b shows nulls and lowered sidelobes in the UC MVDR beampattern (solid magenta) in contrast to the shallow notches and higher sidelobes of the SMI MVDR beampattern (dashed blue).

Algorithm 1 UC MVDR beamformer

procedure SMI MVDR(\mathbf{x})

 \triangleright Compute SMI MVDR weights

$$\mathbf{S} = \frac{1}{L} \sum_{\ell=1}^L \mathbf{x} \mathbf{x}^H$$

$$\mathbf{w}_{SMI} = \mathbf{S}^{-1} \mathbf{v}_0 / (\mathbf{v}_0^H \mathbf{S}^{-1} \mathbf{v}_0)$$

end procedure
procedure PROJECTUNITCIRCLE(\mathbf{w}_{SMI})

 \triangleright Project zeros to unit circle

$$P_S(z) = \mathcal{Z}(\mathbf{w}_{SMI}^H) = G \prod_{n=1}^{N-1} (1 - \xi_n z^{-1})$$

$$\xi_n = r_n e^{j\omega_n}$$

 \triangleright SMI MVDR polynomial zero

if $|\omega_n| > 2\pi/N$ **then**

$$\hat{\xi}_n = e^{j\omega_n}$$

else if $|\omega_n| \leq 2\pi/N$ **then**

$$\hat{\xi}_n = e^{\text{sgn}(\omega_n) j 2\pi/N}$$

end if
end procedure
procedure UC MVDR($\hat{\xi}_n$)

 \triangleright Compute UC MVDR weights

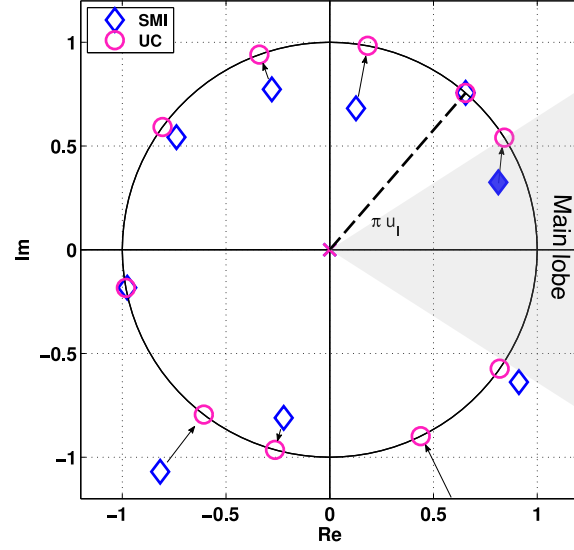
$$P_{UC}(z) = \prod_{n=1}^{N-1} (1 - \hat{\xi}_n z^{-1}) / (1 - \hat{\xi}_n) = \sum_{n=0}^{N-1} c_n^* z^{-n}$$

$$\mathbf{w}_{UC} = [c_1, c_2, \dots, c_N]^T$$

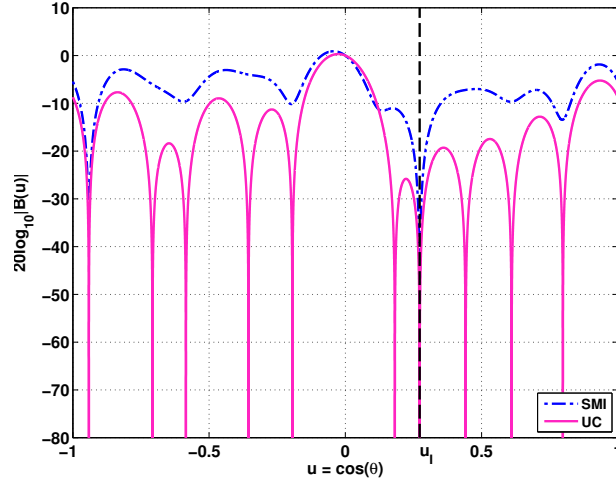
end procedure

V. SIMULATION RESULTS

This section presents results of the simulation experiments evaluating the performance of the UC MVDR beamformer compared to the SMI and the DL MVDR beamformers. All beamformers are implemented using both $N = 11$ and $N = 51$ element ULAs and steered to the broadside look direction ($u_0 = 0$). The experiments assume a passive sonar environment where the beamformers often operate with barely sufficient snapshots $L = N + 1$ and two snapshots per sensor $L = 2N$ is considered a snapshot rich scenario [1], [20]. The desired signal is not present in the snapshots used to estimate the beamformer weights. The assumption of desired signal-free snapshots is commonly used in beamformer design in



(a) Zero locations



(b) Log-magnitude beampattern

Fig. 4. Zero locations and log-magnitude beampatterns of a representative example of SMI MVDR (blue) and UC MVDR ABF (magenta) using $N = 11$ sensor ULA for $L = 12$ snapshots and look direction $u_0 = 0$. The unit circle zeros of the UC MVDR ABF produce nulls and lowers sidelobes compared to the SMI MVDR ABF beampattern.

practical sonar applications [23]. In many passive sonar applications, the beamformers are continuously scanning the observation scene by steering the beampattern across the bearing range. When the beamformer beampattern main lobe is not steered towards any planewave source direction, it is appropriate to model the observed snapshots as signal free.

The simulated snapshots consist of a single loud interferer present at $u_I = 3/N$ and a unit power white background noise. For this measurement scenario, the beamformer output power P_{out} is the sum of the interferer contribution $\mathcal{P}_I = \sigma_I^2 |\mathbf{w}^H \mathbf{v}_I|^2$ and the noise contribution $\mathcal{P}_N = \sigma_W^2 \|\mathbf{w}\|^2$. In the sequel, the two components of the output power are referred to as the interferer output power (\mathcal{P}_I) and white noise output power (\mathcal{P}_N). Sec. V-A compares the interferer output power of the beamformers and Sec. V-B compares the WNGs of the beamformers. Since the white noise output power is determined by the WNG, it is sufficient to compare the beamformer's WNG. All the results are averaged from 3000 Monte Carlo trials.

To ensure a fair comparison between the UC MVDR beamformer and the DL MVDR beamformer, the DL level (δ) can be chosen to match either the average WNGs or the average notch depths (ND) between the two beamformers. In most of the experiments presented, the DL level is chosen to match the

average WNG between the UC MVDR and the DL MVDR beamformer. In order to determine the DL level, the experiments first implement the UC MVDR for all trials and compute the average WNG of the UC MVDR beamformer. The DL level is then estimated iteratively to match the average WNG between the UC MVDR beamformer and the DL MVDR beamformer. In an additional set of experiments, the UC MVDR and DL MVDR performances are compared using the diagonal loading that optimizes SINR per Mestre and Lagunas [24].

A. Interferer output power

Fig. 5 shows the empirical cumulative distribution function (ECDF) of the interferer output power (\mathcal{P}_I) for the UC MVDR beamformer compared to the SMI and DL MVDR beamformers. The upper two panels show the ECDF graphs for the $N = 11$ sensor ULA and the lower two panels show the ECDF graphs for the $N = 51$ sensor ULA. The left two panels show the limited snapshot cases where $L = N + 1$ and the right two panels show the snapshot rich case where $L = 2N$. For all ULA sizes and snapshot cases, the sensor level INR was set at 40 dB. The dashed vertical line represents the ensemble interferer output power P_{ens} obtained from the MVDR beamformer implemented using the ECM. The interferer output power \mathcal{P}_I corresponding to the ECDF equal to 0.5 defines the median output power. The closer the median interferer output power \mathcal{P}_I of the beamformers is to the dashed vertical line, the greater the probability of producing output comparable to the ensemble case. For all four cases examined, the DL level for the DL MVDR beamformer is chosen to match the average WNGs as described earlier.

Over the observed interferer output power range in Fig. 5, the UC MVDR beamformer exhibits higher probability of achieving lower interferer output power \mathcal{P}_I compared against both SMI and DL MVDR beamformers. For instance in Fig. 5a the median output power of UC MVDR was approximately 14 dB lower than SMI beamformer and 10 dB lower than DL MVDR beamformer. The DL MVDR beamformer has improved interferer suppression over SMI beamformer as expected, but the UC MVDR beamformer has improved performance compared to both SMI and DL MVDR beamformers.

Fig. 6 compares the squared mean (solid) and variance (dashed) of interferer output power \mathcal{P}_I for SMI and UC MVDR beamformers over a range of INR values from 0 dB to 40 dB. The interferer output power \mathcal{P}_I of the UC MVDR beamformer has lower mean and variance compared to the interferer output power \mathcal{P}_I of the SMI beamformer. The reduced mean interferer output power \mathcal{P}_I when using the UC MVDR beamformer supports the earlier conclusion that the UC MVDR beamformer provides improved interferer suppression.

B. White noise gain

Fig. 7 compares the WNG of the SMI and UC MVDR beamformers implemented using an $N = 11$ sensor ULA and $L = 12$ snapshots. The maximum possible WNG for this experiment is $WNG = 11$ and corresponds to the CBF [13]. Fig. 7a compares the histograms of the WNG for the SMI and UC MVDR beamformers. The dashed vertical line denotes the ensemble MVDR WNG of 10.473. The UC MVDR beamformer has a greater probability of achieving higher WNG with an average WNG of 5.672 compared to an average WNG of 2.629 using the SMI beamformer.

Fig. 7b is a scatter plot comparing the WNGs for the UC MVDR and the WNG for the SMI beamformers. Each point in the scatter plot denotes the WNG of the UC MVDR beamformer against the WNG of the SMI beamformer for a single realization of the beamformers in the Monte Carlo experiment. The scatter plot shows that the UC MVDR beamformer has a higher WNG than the SMI beamformer in most realizations except for small number of cases (bottom left corner in Fig. 7b) where both beamformers have low WNG. Similar results were observed for the case of $N = 51$ sensor ULA. Thus projecting the sample zeros back to the unit circle frequently but not always improves the WNG from the SMI beamformer. As a result, the average WNG for the UC MVDR beamformer is better than that of the SMI beamformer for the cases examined here.

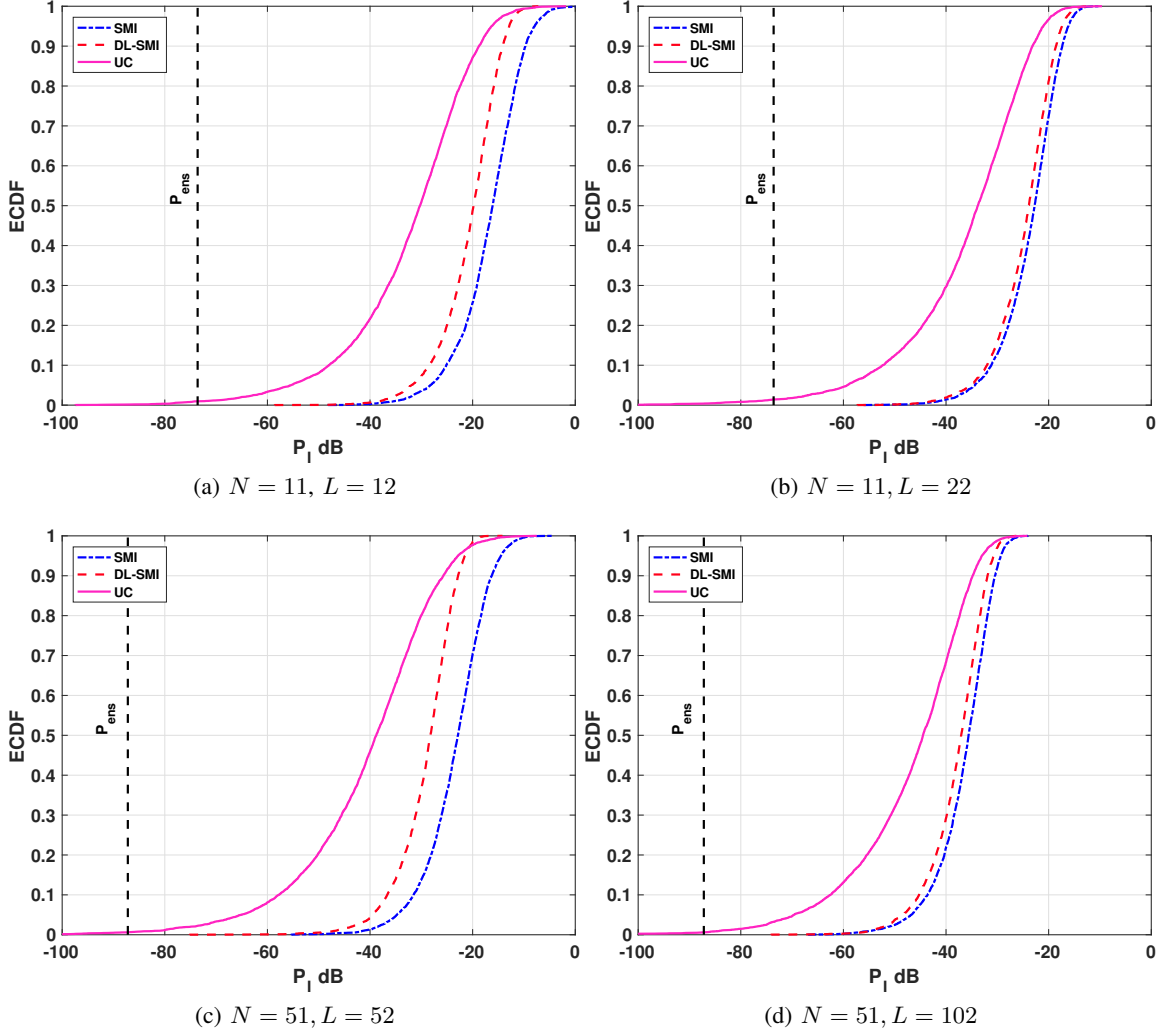


Fig. 5. ECDF of the interferer contributed output power \mathcal{P}_I for the SMI beamformer, the DL MVDR and the UC MVDR beamformer. The beamformers use $N = 11$ element ULA in the top panel and $N = 51$ element ULAs in the bottom panel. The left panels shows the snapshot deficient case ($L = N + 1$) and the right panels shows the snapshot rich case ($L = 2N$). In each panel the dashed vertical line denotes the interferer contributed output power for the ensemble MVDR beamformer. In all cases, the UC MVDR beamformer suppresses the interferer better compared to the SMI and DL MVDR beamformers.

C. UC MVDR and DL MVDR polynomial zeros

The UC MVDR and the DL MVDR beamformer are both derived by modifying the SMI beamformer. As described above, the UC MVDR beamformer moves the sample zeros radially back on to the unit circle. This section discusses how DL changes the DL MVDR zeros and compares this with the UC MVDR polynomial zeros.

Fig. 8 shows array polynomial zeros for a representative example of beamformers implemented using an $N = 11$ element ULA and steered to $u_0 = 0$. A single interferer is present at $u_I = 3/N$ denoted by the radial dashed line. The blue squares denote the sample zeros, the magenta circles denote the UC MVDR zeros and the black diamonds denote the CBF zeros. Each black dot denotes a DL MVDR zero location as the DL level changes from -40 dB to 40 dB in 4 dB steps. When the DL level $\delta = -40$ dB, the DL MVDR zeros are essentially in the sample zero locations. As the DL level increases, the DL MVDR zeros converge towards the CBF zero locations as denoted by the intermediate dot markers. The intermediate dot markers trace a trajectory of DL MVDR zero locations starting from the sample zero location to CBF zero location, as the DL level changes. A specific trajectory is associated with each sample zero. Hence, changing the DL level moves the DL MVDR zeros along specific trajectories. As previously discussed

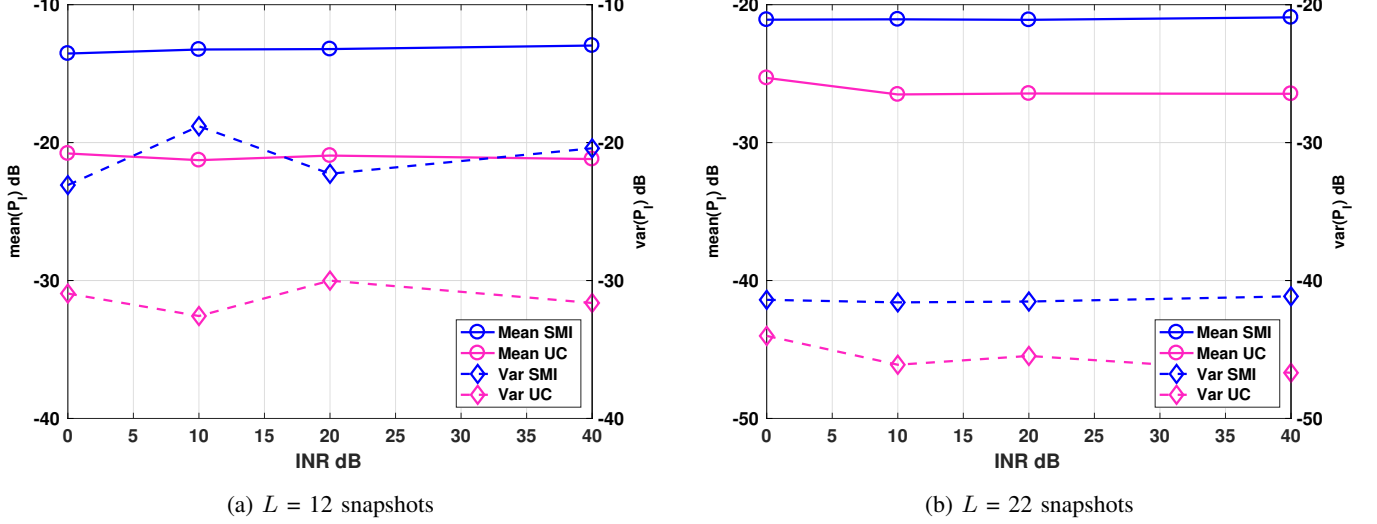


Fig. 6. Dual y-axis plot of mean and variance of interferer output power \mathcal{P}_I for the SMI (blue) and the UC MVDR beamformer (magenta). Both beamformers are implemented using $N = 11$ element ULA and SCM computed from $L = 12$ snapshots in the left panel and $L = 22$ snapshots in the right panel. The UC MVDR beamformer yields interferer contributed output power with lower mean and variance compared to the SMI beamformer.

in Sec. II-A, Mestre and Lagunas present an approach to compute the optimal DL level [24]. The DL MVDR zeros associated with the optimal DL level are still constrained on the specific trajectories of each sample zero, and may not be particularly close to the ensemble zero locations. Comparatively, the UC MVDR beamformer uses a markedly different approach by moving the sample zeros radially back to the unit circle.

Moreover, one advantage of DL is that it improves the WNG of the beamformers [13]. As the DL MVDR zeros move closer to the CBF zero locations, the WNG performance improves. However, moving zeros closer to the CBF zero locations leads to loss of ND in the interferer direction. Hence choosing the DL level involves a trade off between loss of interferer suppression and improved WNG. By moving the zeros to the unit circle, the UC MVDR creates beampattern nulls, which improve the interferer suppression compared to DL MVDR, and as a by-product often improves WNG as well. Further, the UC MVDR beamformer does not require choosing a tuning parameter like the DL level.

Fig. 9 compares the mean interferer contributed output power for the UC MVDR (magenta diamonds) and the optimal DL MVDR (red circles) beamformers for a range of snapshot values $12 \leq L \leq 22$. The optimal DL level is computed using the approach detailed in [24], assuming the knowledge of the ECM. The horizontal solid line denotes the interferer contributed output power for the ensemble MVDR beamformer. The beamformers are implemented using an $N = 11$ sensor ULA and steered towards broadside look direction ($u_0 = 0$). A single interferer with $\text{INR} = 40$ dB is present at $u_I = 3/N$. Comparing the output powers shows that the UC MVDR beamformer suppresses the interferer better than optimal DL MVDR beamformer over a range of snapshot values. As discussed earlier, applying DL moves the sample zeros away from the ensemble locations and towards the CBF locations. As a result the optimal DL MVDR is improving the WNG at the expense of interferer suppression.

The improved interferer suppression of the UC MVDR beamformer in Fig. 9 is impressive in light of the asymmetrical information between the beamformers in favor of the DL MVDR beamformer. The DL MVDR beamformer has perfect knowledge of the ECM to compute the optimal DL, which is then used to process SCM data for the performance plotted in Fig. 9. In contrast, the UC MVDR is operating only with SCM data. The UC MVDR beamformer rejects interferers better than the DL MVDR even when the latter beamformer has access to perfect information for optimizing the DL level.

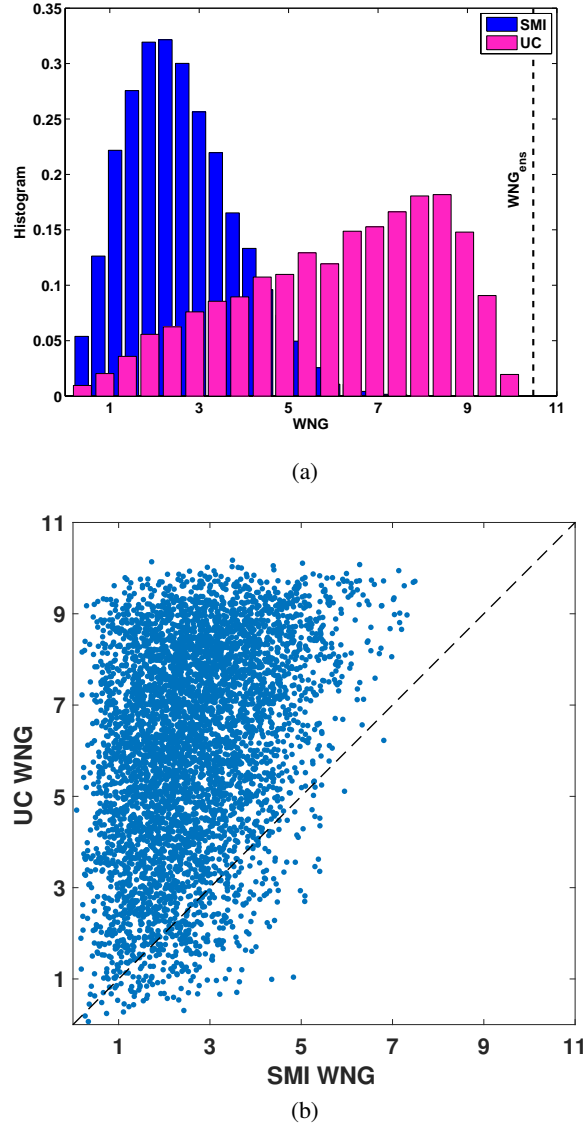


Fig. 7. Comparison of WNG for the UC MVDR and the SMI beamformer, both implemented using an $N = 11$ element ULA and $L = 12$ snapshots. The top panel compares the histogram of WNGs and the lower panel is a scatter plot of the WNGs. On average, the UC MVDR beamformer has higher WNG compared to the SMI beamformer.

VI. DISCUSSION

This paper seeks to identify the value of the UC rectification process, which is most clearly displayed in isolation separate from other rectification or regularization techniques. As such, the only main-lobe protection incorporated in the UC MVDR beamformer is the zero exclusion described in Sec. IV. In practice, the UC rectification would likely be combined with other covariance matrix and array weight conditioning techniques such as Toeplitz rectification [2], [4], [6], diagonal loading [13], [31], or limiting the white noise gain [7]. Incorporating one or more of these techniques into our initial exploration of the algorithm might obscure the value of the UC rectification process. In isolating the UC rectification, we established the value of this technique in suppressing discrete interferers and often attenuating white noise as well. Future work can progress to more complicated issues such as the interactions of UC rectification with the covariance matrix conditioning techniques listed above.

The proposed UC rectification algorithm excludes zeros within the null-to-null main-lobe width to prevent main-lobe distortion. This approach prevents the UC MVDR beamformer from suppressing discrete interferers inside the main-lobe. There are several promising candidates for protecting the main-lobe while

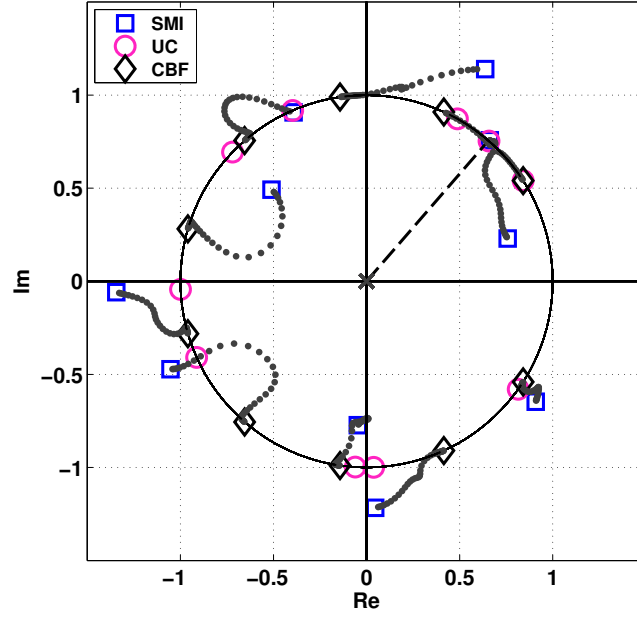


Fig. 8. UC MVDR polynomial zeros compared against DL MVDR polynomial zeros as the DL level δ is increased from -40 dB to 40 dB. The DL MVDR polynomial zeros asymptotically converge to CBF polynomial zero locations as $\delta \rightarrow \infty$.

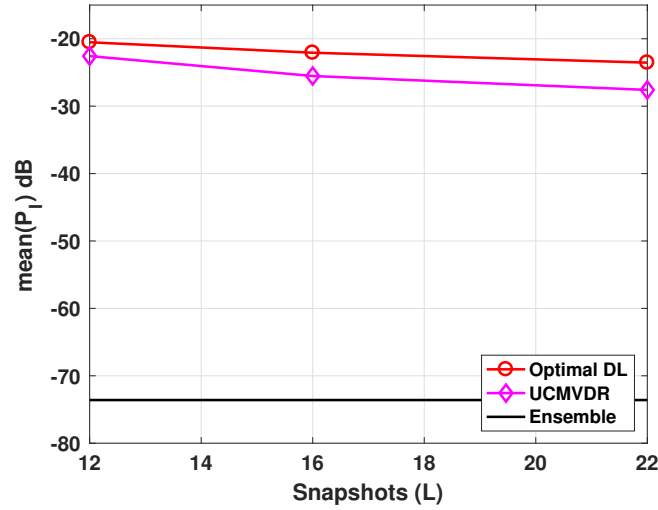


Fig. 9. Interferer output power for the UC MVDR and the optimal DL MVDR beamformers for a range of snapshot values $12 \leq L \leq 22$. The horizontal solid line denotes the interferer output power for the ensemble MVDR beamformer. The beamformers are implemented using an $N = 11$ sensor ULA and steered towards broadside look direction ($u_0 = 0$). A single interferer with $\text{INR} = 40$ dB is present at $u_I = 3/N$. The UC MVDR beamformer suppresses the interferer better than the optimal DL MVDR beamformer whose DL level is computed using the knowledge of the ECM.

suppressing main-lobe interferers using the UC MVDR beamformer. First, one could make the exclusion zone narrower around the look direction. Instead of excluding zeros within the null-to-null main-lobe width, one might only exclude them within the half power main-lobe width, sacrificing some WNG to suppress a loud interferer approaching the look direction. This approach is analogous to varying the inner product threshold in [28]. Another approach could introduce a constraint on the radius of the projected zeros within the main-lobe. The sample zeros within the main-lobe width would be radially projected towards the unit circle, but stop short of the unit circle based on a constraint on the WNG. This would create notches near the main-lobe interferers and produce smaller values of ND compared to the current

formulation of the UC MVDR beamformer.

The UC MVDR beamformer uses radial projection as the simplest method for UC rectification comparable to Cadzow's the diagonal averaging approach as the simplest method to project the SCM to the nearest Toeplitz matrix [2]. Subsequent authors [3], [4], [6] developed more complicated maximum likelihood estimation algorithms for finding the most likely Toeplitz matrix, usually much more complicated than the diagonal averaging. We anticipate future refinements on the UC rectification exploiting progress establishing the distribution of the sample zeros as in Fig. 2 will likewise produce more sophisticated ML estimates of zeros projected onto the unit circle. However, the highly nonlinear and at times poorly conditioned nature of polynomial roots may make this more challenging than Toeplitz rectification [2]–[4] or optimizing diagonal loading [21], [32].

An important open challenge remains to find the probability distribution of the sample zeros perturbations away from the ensemble locations on the unit circle due to limited sample support and possibly also array element mismatch [33]. This is a challenging problem even for a second order polynomial, the distribution of the roots of quadratic as given by quadratic formula can be very complicated from the distributions of the polynomial coefficients. The complexity of this nonlinear mapping of probability distributions of the coefficients to probability distributions of the roots is beyond the scope of this paper, but when solved will resolve many of the open issues above. It would be a significant step to prove that the distribution of the perturbations of the zeros is circularly symmetric under some conditions. The scatter plots of Fig. 2 tempt us to conjecture this must be the case for at least some problems, but we have not proven it at this point in time. If the perturbation distribution is circularly symmetric, depending only on the radius of the perturbation and not the angle, the radial projection back to the unit circle may well prove to be a maximum likelihood estimate by minimizing the radius.

VII. CONCLUSION

This paper proposed the UC MVDR beamformer which projects the SMI MVDR array polynomial zeros radially to the unit circle to create perfect notches in the beampattern. By moving the sample zeros to the unit circle, the UC MVDR zeros satisfy the unit circle property on the ensemble zeros. Numerical simulations verify that the UC MVDR beamformer often simultaneously improves interferer suppression and WNG compared to the SMI MVDR ABF. By moving the zeros onto the unit circle, the UC MVDR is able to suppress interferers better than the optimal DL MVDR whose DL factor is computed using perfect knowledge of the ECM. Unlike DL MVDR, the UC MVDR does not require an *a priori* choice of parameter to achieve this improvement in performance.

APPENDIX A

PROOF OF UNIT CIRCLE PROPERTY ON ENSEMBLE MVDR ARRAY POLYNOMIAL ZEROS

The ensemble MVDR array polynomial zeros must be located on the unit circle for planewave beamforming using ULA. Steinhardt and Guerci proved this property of the MVDR ensemble zeros in [10], but the result does not appear to be widely known. The proof below closely follows the Steinhardt and Guerci proof by contradiction.

The MVDR weight vector \mathbf{w}_{MVDR} solves the optimization problem in (4). The quadratic objective function in (4) is a convex function in \mathbf{w} because the ECM is a positive-definite matrix [13]. This convexity implies a unique solution exists for (4). The objective function can be expressed in terms of the ensemble spatial power spectrum $S(u)$ and MVDR beampattern

$$f(\mathbf{w}) = \frac{1}{2} \int_{-1}^1 S(u) |B(u)|^2 du. \quad (10)$$

Note that (10) is a Parseval's relation equating the energy evaluated in the spatial frequency domain to the energy evaluated in the spatial domain in (4).

Replace the beampattern with MVDR polynomial $P_M(z = e^{j\pi u})$ to get

$$f(\mathbf{w}) = \int_{-1}^1 S(u) |P_M(e^{j\pi u})|^2 du. \quad (11)$$

The zero locations correspond to the MVDR weights. Factor the polynomial for the solution of (4) as

$$P_M(e^{j\pi u}) = \prod_{n=1}^{N-1} \frac{(1 - \zeta_n e^{-j\pi u})}{(1 - \zeta_n^*)} \quad (12)$$

where ζ_i s are the ensemble MVDR zeros and $P_M(z) = 1$ for $z = 1$. Using (12) in (10), the objective function is

$$f(\mathbf{w}_{\text{MVDR}}) = \frac{1}{2} \int_{-1}^1 S(u) \prod_{n=1}^{N-1} \frac{(1 - \zeta_n e^{-j\pi u})}{(1 - \zeta_n^*)} \frac{(1 - \zeta_n^* e^{j\pi u})}{(1 - \zeta_n)} du \quad (13)$$

Assume the zeros in (12) are not on the unit circle. Replacing one zero ζ_i by its conjugate-reciprocal $1/\zeta_i^*$ in (13) leaves the objective function unchanged. However, changing the zero alters the polynomial $P_M(z)$ resulting in a different weight vector. This implies there exists a weight vector different from the weight vector corresponding to (12) which still optimizes (4). This contradicts with the uniqueness of the solution to (4). The uniqueness holds only when the zeros of $P_M(z)$ are on the unit circle. Hence the MVDR zeros must be on the unit circle.

REFERENCES

- [1] A. B. Baggeroer and H. Cox, "Passive sonar limits upon nulling multiple moving ships with large aperture arrays," *Conference Record of the Thirty-Third Asilomar Conference on Signals, Systems, and Computers*, vol. 1, pp. 103–108, Nov. 1999.
- [2] J. Cadzow, "Signal enhancement using canonical projection operators," in *1987 IEEE International Conference on Acoustics, Speech, and Signal Processing*, vol. 12, Apr 1987, pp. 673–676.
- [3] T. A. Barton and S. T. Smith, "Structured covariance estimation for space-time adaptive processing," in *1997 IEEE International Conference on Acoustics, Speech, and Signal Processing*, vol. 5, Apr 1997, pp. 3493–3496 vol.5.
- [4] P. Vallet and P. Loubaton, "Toeplitz rectification and DOA estimation with MUSIC," in *2014 IEEE International Conference on Acoustics, Speech and Signal Processing (ICASSP)*, May 2014, pp. 2237–2241.
- [5] —, "On the performance of MUSIC with Toeplitz rectification in the context of large arrays," *IEEE Transactions on Signal Processing*, vol. 65, no. 22, pp. 5848–5859, 2017.
- [6] D. R. Fuhrmann, "Application of Toeplitz covariance estimation to adaptive beamforming and detection," *IEEE Journal of Selected Topics in Signal Processing*, vol. 39, no. 10, pp. 2194–2198, Oct. 1991.
- [7] H. Cox, R. Zeskind, and M. Owen, "Robust adaptive beamforming," *IEEE Transactions on Acoustics, Speech, and Signal Processing*, vol. 35, no. 10, pp. 1365–1376, Oct. 1987.
- [8] E. N. Gilbert and S. P. Morgan, "Optimum design of directive antenna arrays subject to random variations," *Bell System Technical Journal*, vol. 34, no. 3, pp. 637–663, May 1955.
- [9] J. Capon, "High-resolution frequency-wavenumber spectrum analysis," *Proceedings of the IEEE*, vol. 57, no. 8, pp. 1408–1418, Aug. 1969.
- [10] A. Steinhardt and J. Guerci, "STAP for RADAR: what works, what doesn't, and what's in store," in *Proceedings of the IEEE Radar Conference*, Apr. 2004, pp. 469–473.
- [11] S. Schelkunoff, "Mathematical theory of linear arrays," *Bell System Technical Journal*, vol. 22, no. 1, pp. 80–107, Jan. 1943.
- [12] S. R. Tuladhar and J. R. Buck, "Unit circle MVDR beamformer," in *2015 IEEE International Conference on Acoustics, Speech and Signal Processing (ICASSP)*, April 2015, pp. 2484–2488.
- [13] H. L. Van Trees, *Detection, Estimation, and Modulation Theory, Optimum Array Processing*. New York: John Wiley & Sons, 2002.
- [14] D. H. Johnson and D. E. Dudgeon, *Array Signal Processing: Concepts and Techniques*. New York: Simon & Schuster, 1992.
- [15] D. M. Boroson, "Sample size considerations for adaptive arrays," *IEEE Transactions on Aerospace and Electronic Systems*, vol. 16, no. 4, pp. 446–451, Jul. 1980.
- [16] I. S. Reed, J. D. Mallett, and L. E. Brennan, "Rapid convergence rate in adaptive arrays," *IEEE Transactions on Aerospace and Electronic Systems*, vol. 10, no. 6, pp. 853–863, Nov. 1974.
- [17] H. Cox, "Multi-rate adaptive beamforming (MRABF)," in *Proceedings of the 2000 IEEE Sensor Array and Multichannel Signal Processing Workshop*, Cambridge, MA, Mar. 2000, pp. 306–309.
- [18] B. Carlson, "Covariance matrix estimation errors and diagonal loading in adaptive arrays," *IEEE Transactions on Aerospace and Electronic Systems*, vol. 24, no. 4, pp. 397–401, Jul. 1988.
- [19] C. D. Richmond, "MVDR adaptive sidelobes: Extending Ruze's formula and providing an exact calculation of the probability of sidelobe suppression," in *Sensor Array and Multichannel Signal Processing Workshop*, Cambridge, MA, Mar. 2000, pp. 73–76.

- [20] H. Cox, "Adaptive beamforming in non-stationary environments," *Conference Record of the Thirty-Sixth Asilomar Conference on Signals, Systems and Computers*, vol. 1, pp. 431–438, Nov. 2002.
- [21] X. Mestre and M. A. Lagunas, "Diagonal loading for finite sample size beamforming: an asymptotic approach," in *Robust Adaptive Beamforming*. New York: John Wiley and Sons, 2005.
- [22] R. R. Nadakuditi and A. Edelman, "The bias of the MVDR beamformer outputs under diagonal loading," in *IEEE International Conference on Acoustics, Speech, and Signal Processing*, vol. 4. IEEE, 2005, pp. 793–796.
- [23] A. Gershman, "Robust adaptive beamforming: An overview of recent trends and advances in the field," in *4th International Conference on Antenna Theory and Techniques, 2003.*, vol. 1. Sevastopol, Ukraine: IEEE, Sep. 2003, pp. 30–35.
- [24] X. Mestre and M. A. Lagunas, "Finite sample size effect on minimum variance beamformers: optimum diagonal loading factor for large arrays," *IEEE Transactions on Signal Processing*, vol. 54, no. 1, pp. 69–82, Jan. 2006.
- [25] B. D. Steinberg, *Principles of Aperture and Array System Design: Including Random and Adaptive Arrays*. New York: John Wiley & Sons, 1976.
- [26] A. V. Oppenheim and R. W. Schaffer with J. R. Buck, *Discrete-Time Signal Processing*, 2nd ed. Englewood Cliffs, NJ: Prentice-Hall, 1999.
- [27] C. Richmond, "Statistics of adaptive nulling and use of the generalized eigenrelation (GER) for modeling inhomogeneities in adaptive processing," *IEEE Transactions on Signal Processing*, vol. 48, no. 5, pp. 1263–1273, May 2000.
- [28] H. Cox and R. Pitre, "Robust dmr and multi-rate adaptive beamforming," in *Signals, Systems & Computers, 1997. Conference Record of the Thirty-First Asilomar Conference on*, vol. 1. IEEE, 1997, pp. 920–924.
- [29] H. Cox, R. Pitre, and H. Lai, "Robust adaptive matched field processing," in *Conference Record of Thirty-Second Asilomar Conference on Signals, Systems and Computers (Cat. No.98CH36284)*, vol. 1, Nov 1998, pp. 127–131 vol.1.
- [30] S. M. Kogon, "Robust adaptive beamforming for passive sonar using eigenvector/beam association and excision," in *Sensor Array and Multichannel Signal Processing Workshop Proceedings, 2002*, Aug 2002, pp. 33–37.
- [31] C. J. Ryan and J. R. Buck, "Applying the unit circle constraint to the diagonally loaded minimum variance distortionless response beamformer," in *2017 IEEE International Conference on Acoustics, Speech and Signal Processing (ICASSP)*, March 2017, pp. 3366–3369.
- [32] M. Pajovic, "The development and application of Random Matrix Theory in adaptive signal processing in the sample deficient regime," Ph.D. dissertation, Woods Hole Oceanographic Institution/Massachusetts Institute of Technology, 2014.
- [33] C. J. Ryan, "The unit circle diagonally loaded MVDR beamformer and a perturbation analysis of practical adaptive beamformers," Master's thesis, University of Massachusetts Dartmouth, 2017.